Developing a low cost multipurpose X-band FMICW radar

Journal of the European Ceramic Society 45 (2025) 117231

Contents lists available at ScienceDirect

Journal of the European Ceramic Society

journal homepage: www.elsevier.com/locate/jeurceramsoc

Titanium-based brazing alloy for bonding oxide/oxide CMCs for steelmaking industry applications

Carla Malinverni [a,*], Valentina Casalegno [a], Pierre Bertrand [b], Georg Puchas [c], Stefan Schafföner [c], Milena Salvo [a]

[a] Department of Applied Science and Technology, Politecnico di Torino, Corso Duca degli Abruzzi 24, Torino 10129, Italy
[b] UTBM, CNRS, Laboratory ICB, UMR - 6303 CNRS, Belfort 90010, France
[c] Chair of Ceramic Materials Engineering, University of Bayreuth, Prof.-Rüdiger-Bormann-Str. 1, Bayreuth 95447, Germany

ARTICLE INFO

Keywords:
Joining, Brazing
High-entropy alloy
Ceramic matrix composite
Oxide/oxide fiber composites

ABSTRACT

In this work, a Ti-based high-entropy alloy was used to join Al_2O_{3f} / Al_2O_3-ZrO_2 ceramic matrix composites, intended for use as radiant tube furnace components in energy-intensive industries such as steelmaking. The brazing cycle was conducted in a vacuum tubular furnace up to 1050 °C. The brazing material consisted of brazing alloy powders mixed with a water-based binder. Process parameters studied included the weight percentages of the binder, the pressure applied on the joints, and additional heat treatments to obtain successful brazed CMCs. Morphological characterizations were conducted to analyze the brazed joints and the microstructure of the filler metal. Mechanical shear tests at room temperature were performed to assess the apparent shear strength of the brazed joints, measuring 49 ± 8 MPa of apparent shear strength for butt-configuration joints with failure mode caused by the delamination of the composite. Additionally, direct-flame exposure tests were conducted to evaluate the brazed joints in combustion environments.

1. Introduction

In recent years, ceramic matrix composites (CMCs) have gained significant importance in industrial applications compared to monolithic ceramics due to their unique properties. They are characterized by high heat resistance, hardness, corrosion resistance and high damage tolerance [1,2]. These characteristics enable them to maintain excellent thermo-mechanical properties in challenging conditions that can be found in industries such as aerospace [3], automotive [4], concentrated solar power [5], as well as in the energy-intensive steelmaking sector, where CMCs can replace standard materials used for radiant tubes, such as Inconel alloys and stainless steel. The main drawback of stainless steel is that it cannot withstand the required operating conditions in modern steelmaking due to the presence of biogas mixtures. However, biogas is necessary to employ cleaner production technologies and to reduce CO_2 emissions. Furthermore, materials with higher corrosion resistance are necessary in steelmaking to increase the processing efficiency and to extend the life of the components.

Successful solutions for joining ceramic matrix composites are essential since the manufacturing of large and complex CMC components is difficult and expensive [6–8]. Among different joining methods for CMC, brazing [9–11], glass-ceramic joining [12], the application of a partial transient liquid phase [13], diffusion bonding [14] and reaction forming [15] can be listed as some of the most widely investigated methods. In the case of oxide-based CMCs, to the best of the authors' knowledge, not many solutions can be found [16–18]. Particularly, high-entropy alloys (HEAs) were proposed as joining and brazing materials for CMCs [5,19–24]. HEAs applied for joining are characterized by a relatively low brazing temperature while maintaining a high operating temperature [25]. This makes them suitable for the joining of superalloys, refractory metals and carbon fiber composites in many industrial applications [26–28].

Apart from their beneficial processing, HEAs are used as joining materials due to several advantageous properties they possess [29]. HEAs often exhibit superior mechanical properties such as high strength, hardness, toughness and thermal stability. This makes them ideal for joining applications where the joint needs to withstand significant mechanical loads. This is also particularly important in high-temperature applications, where the joint material must endure thermal cycles without degrading. Thus, HEAs are good candidates as joining materials

* Corresponding author.
E-mail address: carla.malinverni@polito.it (C. Malinverni).

https://doi.org/10.1016/j.jeurceramsoc.2025.117231
Received 14 October 2024; Received in revised form 19 December 2024; Accepted 20 January 2025
Available online 21 January 2025

for CMCs since they typically exhibit enhanced resistance to corrosion and oxidation, ensuring that the joints are more durable and reliable in harsh environments. Additionally, the composition of HEAs can be tailored to achieve specific properties, allowing for customization based on the requirements of the joining application. Nevertheless, the design of the composition of HEAs should result in a homogeneous element distribution and uniform microstructure to optimize their mechanical properties, corrosion resistance, and structural integrity [30,31].

Previous studies demonstrated the potential of HEAs containing titanium as a joining material for advanced brazing applications. One noteworthy study [32] explored the use of a high-entropy TiZrHfNbMo alloy for brazing Si_3N_4 ceramics. It was demonstrated that the TiZrHfNbMo alloy forms robust metallurgical bonds with the ceramic, resulting in strong joints. The interfacial microstructure typically included layers such as Ti_5Si_3 and various Cu-Ti intermetallic compounds. Optimal brazing temperatures were found to be around 820–840 °C and the shear strength of the joints reached up to 86 MPa. Another research work [33] involved designing a TiZrCuNiAg brazing filler metal for titanium alloys, highlighting the versatility of titanium in brazing applications, which showed promising results for creating strong joints.

In this work, a titanium-based high-entropy alloy was used to braze oxide-based CMCs, which are required to resist operating temperatures up to 900 °C and face combustion, with a minimum joint strength of 15 MPa. Brazing process parameters were optimized to obtain successfully brazed CMCs. The microstructure of the joints was characterized by scanning electron microscopy and they were mechanically tested at room temperature to measure the apparent shear strength and failure mode. Direct flame exposure tests with C_2H_2/O_2 flame were also performed at 900 °C on the brazed joints in both flat- and butt-configurations to replicate in-service conditions present in combustion environments.

2. Materials and methods

2.1. Oxide-based ceramic matrix composites

Oxide-based ceramic matrix composites (oxide/oxide CMCs) used in this work consisted of an alumina-zirconia matrix reinforced with eight layers of Nextel™ 610 alumina fiber fabric DF-19 (3 M, USA). This oxide/oxide CMC is characterized by a high flexural strength, chemical stability at high temperatures thanks to its intrinsic oxidation resistance, and considerable fracture toughness due to the crack deflection mechanisms typical of weak matrix composites. The oxide/oxide CMC was provided in the form of a 100 mm × 100 mm × 3 mm plate. It was manufactured following the process described in a previous study [34]. The plate was cut using a precision cutting machine to obtain oxide/-oxide CMC substrates of around 15 mm × 10 mm × 3 mm for the subsequent joining experiments. The interlaminar shear strength (ILSS) of the oxide/oxide CMC was 12 MPa. The coefficient of thermal expansion of the composite was determined with $8.3{\cdot}10^{-6}$ K^{-1} (200°C – 600°C) [35].

2.2. Titanium-based brazing alloy as filler metal

The brazing alloy used in this work was a high-entropy alloy with the tradename TiBraze200Nb, which was supplied by Titanium Brazing Inc., USA. This alloy was supplied in the form of powders with particle size of – 140 mesh (maximum particle size dimension of 106 μm) with a water-based gel binder. The TiBraze200Nb powder was manufactured as a mixture of the TiBraze200 brazing alloy from the same company with the addition of Nb powder [27], a refractory element that is added to increase the heat resistance of the brazed joints [36,37]. Important metallurgical properties of the TiBraze200Nb brazing alloy are summarized in Table 1.

Before the brazing process, the oxide/oxide CMCs were cleaned with ethanol and sonicated in an ultrasonic bath to remove any impurities or contaminants on the surface. A clean brazing surface is crucial before joining to promote capillary attraction, since any contamination on the surfaces may lead to gaps between the brazing and the substrate, which decrease the joint properties. The preparation of the brazing paste consisted of selecting the optimal weight percentage of the water-based gel binder to add to the brazing powder. 16 wt% binder was mixed with the TiBraze200Nb powders to obtain a paste with homogeneous consistency and uniform spreadability on the CMC's surface, while still remaining a low amount of binder to avoid porosity formation caused by the debinding during the subsequent heat treatment. The paste obtained was spread with a spatula onto one of the oxide/oxide substrates, while another CMC substrate was placed on top afterwards, thus obtaining a sandwich-like structure. As can be seen from Fig. 1, flat-joint and butt-joint configurations were chosen as the two configurations of brazed joints, distinguished by the different orientations of the CMC's surface in relation to the brazing area.

The flat-joints were characterized by having the 2D fiber architecture parallel to the brazing area, while the butt-joints had fiber bundles perpendicular to the brazing area, providing information about the behavior of the brazing alloy along the alumina fibers. After preparing the samples, they were held at room temperature for around 15–20 h to let the brazing paste dry. The assembled samples were then subjected to an optimized thermal treatment conducted in a vacuum tubular furnace (RHTH 70–150/16, Nabertherm, Germany) equipped with a rotary pump and a turbomolecular pump, reaching a vacuum pressure of 10^{-5} mbar for the whole duration of the brazing cycle. The typical thickness of the brazing seam obtained was in the range of 300–400 μm. The brazing process consisted of four steps. Fig. 2 shows the brazing cycle performed, which was recommended by the brazing alloy manufacturer, with subsequent optimization of the parameters (temperatures and times) to find the most suitable compromise.

The first dwell time of 20 min at 750 °C, reached with a heating rate of 480 K/h, ensured an even temperature distribution inside the vacuum chamber and minimized the decrease of the vacuum that occurs between 400-650 °C due to evaporation of the binder degradation products. The second dwell time of 10 min was set at the brazing temperature of 1050 °C, which was above the liquidus temperature of the alloy. This was followed by an annealing at 900 °C for 2 h, which was conducted to promote the Nb diffusion along the brazing seam to improve the heat resistance of the resulting brazed joints. Finally, to release thermo-mechanical stresses, thereby avoiding the formation of cracks in the brazed joints, a last dwell step was conducted at 700 °C for 20 min, followed by a cooling to room temperature with a cooling rate of 300 K/h.

To verify the compatibility between the TiBraze200Nb brazing alloy and the oxide/oxide CMC, preliminary joints were prepared with the brazing cycle shown in Fig. 2 using monolithic Al_2O_3 substrates (HESSE Instruments, Germany) without any applied pressure.

Subsequently, the effect of the applied pressure on the oxide/oxide CMC joints during the brazing cycle was investigated. In particular, tungsten weights were placed on top of the assemblies and they were adjusted to give 2 kPA for both butt- and flat-configuration joints. They were used to provide compression during heating and brazing and to

Table 1
Properties of TiBraze200Nb brazing alloy used as filler metal to join oxide/oxide CMCs [27].

Tradename	Composition [wt%]	Solidus temperature [°C]	Liquidus temperature [°C]	Brazing temperature [°C]
TiBraze200Nb	Ti−17Zr−17Cu−17Ni−17Nb	848	1020	1030–1100

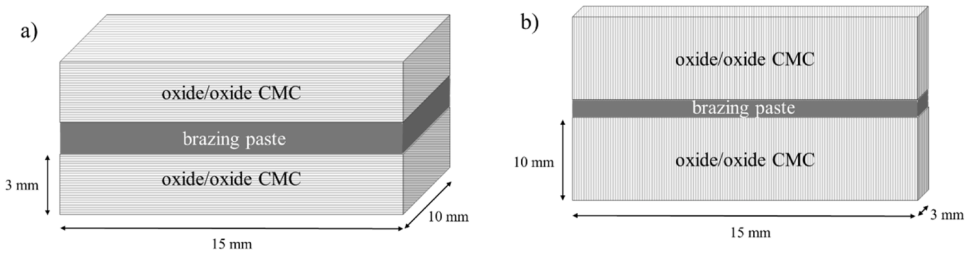

Fig. 1. Schematic representation of flat-joint (a) and butt-joint (b) using brazing alloy paste as filler metal.

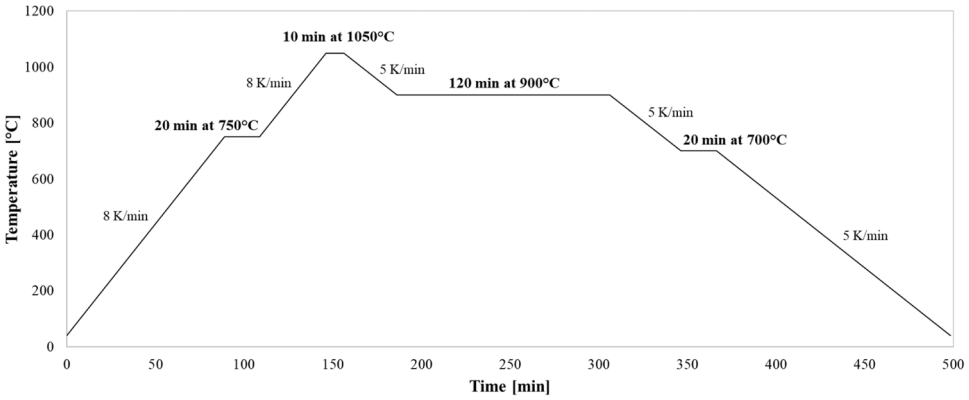

Fig. 2. Brazing cycle for oxide/oxide CMCs joined with TiBraze200Nb brazing paste as filler metal.

improve the adhesion at the interface of the TiBraze200Nb brazing paste with the two CMC substrates.

The microstructure and the elemental analysis of the joints obtained were characterized using high-resolution field emission scanning electron microscopy, together with energy dispersive X-ray spectrometry for quantitative analysis and elemental mapping (FESEM Supra TM 40, ZEISS, Germany).

Mechanical characterization using single lap offset (SLO) tests under compression was performed to measure the apparent shear strength of joints obtained in flat- and butt-configuration. These SLO tests were carried out at room temperature using a universal testing machine (SINTEC D/10, Germany), according to a method adopted from standard the ASTM D905–08, with a crosshead speed of 0.5 mm/min and a 50 kN load cell. The apparent shear strength of the joints was measured by dividing the maximum load by the brazing area, and the mean value ± standard deviation was reported. The set-up for SLO testing was reported in previous studies [35]. For these tests, the joined area was determined on the fractured joint surfaces after the SLO measurements and resulted in around 10 mm × 10 mm for flat-joints and around 10 mm × 3 mm for butt-joints. Furthermore, X-ray computed tomography (CT-scan, Fraunhofer IKTS, Germany) with an open microfocus X-ray tube (filament voltage 180 kV, current 90 μA, exposure time 1 s, 0.2 mm Cu filter) was performed on a flat-joint to study and evaluate the interface of the brazing alloy to the composite, especially regarding the formation of porosities in the brazing seam.

To simulate the behaviour of the brazing material in a combustion environment, the joints were exposed to an acetylenic oxy-fuel flame with a stoichiometric composition, as illustrated in Fig. 3. The distance between the flame and the side exposed to the combustion gases was adjusted to achieve a temperature of 900 °C on the samples' surface. This temperature was monitored by a two-colour pyrometer and a thermal imaging camera directed toward the area of the brazed joints. For the flat- and butt-joint configuration, direct flame exposure tests were carried out at the edge of the joints to test directly the joining material between the two composite components. In this configuration, the temperature of 900 °C was reached on the face exposed to the flame, although a thermal gradient was present in the depth of the samples, minimizing the thermal effect on the brazed joint.

3. Results and discussion

Preliminary brazed joints were prepared with monolithic Al_2O_3 and a binder percentage between 14 and 16 wt%, and their cross-section is shown in Fig. 4.

The SEM cross-section showed a good and homogeneous interface proving an excellent compatibility of the TiBraze200Nb brazing paste and the alumina substrate. Even so, some pores were present along the brazing seam.

The brazing cycle was subsequently performed on the oxide/oxide CMCs in both joint configurations placing a tungsten weight during the brazing heat treatment.

The cross-sections of the typical brazed flat-joint obtained are shown

Fig. 3. Direct flame exposure test on flat configuration joint.

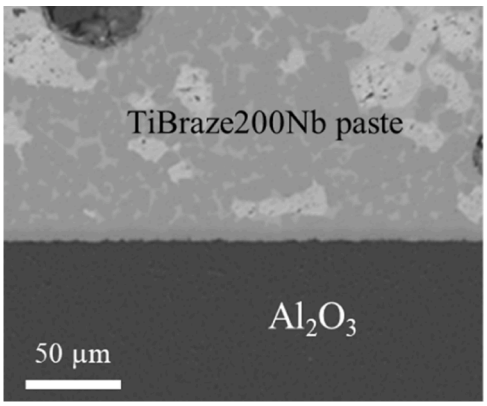

Fig. 4. Brazing of Al_2O_3 bulk substrates with TiBraze200Nb paste as the brazing filler metal. The interface with the alumina substrate appears homogeneous.

in Fig. 5, in which some large pores were detected along the brazing seam. In particular for flat-joint samples, the interface between the brazing material and the alumina fibers appeared better than the interface between brazing material and the composite matrix, which seemed slightly detached. In Fig. 4b it can be noticed that the brazing alloy infiltrated the composite matrix porosity due to capillarity.

For the butt-configuration, the cross-sections of a typical brazed joint obtained are shown in Fig. 6. The composite/braze interfaces were continuous, no detachments were observed, and the braze had a homogeneous microstructure and a relatively low porosity. The infiltration of the brazing alloy can be seen along the fibers perpendicular to the joined area, which was much more pronounced compared to the flat joint counterpart. This indicated the formation of an interlocked structure which can promote adhesion at the braze/composite interface and increase the mechanical strength.

The mechanical interlocking created between the alumina fibers and the alloy provided a very sound joint. Even though, the challenging preparation of the joints in this configuration due to the associated smaller joint area (Fig. 1b) resulted in an uneven thickness of the brazing seam across the joint, as shown in Fig. 6a.

The microstructural analysis revealed that the interface between the TiBraze200Nb and the base material was particularly good in fiber bundle areas (Fig. 6). The poorer wetting behavior of the brazing alloy at the interface with the composite in flat-joint configuration (Fig. 5) is speculated to be attributed to the presence of ZrO_2 in the composite matrix, which exhibits poor wettability by molten Ti, Ni, and Cu [38, 39].

EDX elemental mapping was performed to study the microstructure of the brazing alloy after the brazing cycle. The maps obtained are reported in Fig. 7.

All the elements of the HEA were widely distributed across the joint seam. The FESEM magnified view of the joint area as reported in Fig. 7a displays the microstructure of the brazing seam. In the images are indicated by four different areas (A, B, C and D) that were found in the TiBraze200Nb microstructure. In the brazing paste, niobium is the element with the highest atomic weight, which resulted in the bright niobium-rich phase (Fig. 7f). The role of Nb was previously studied in

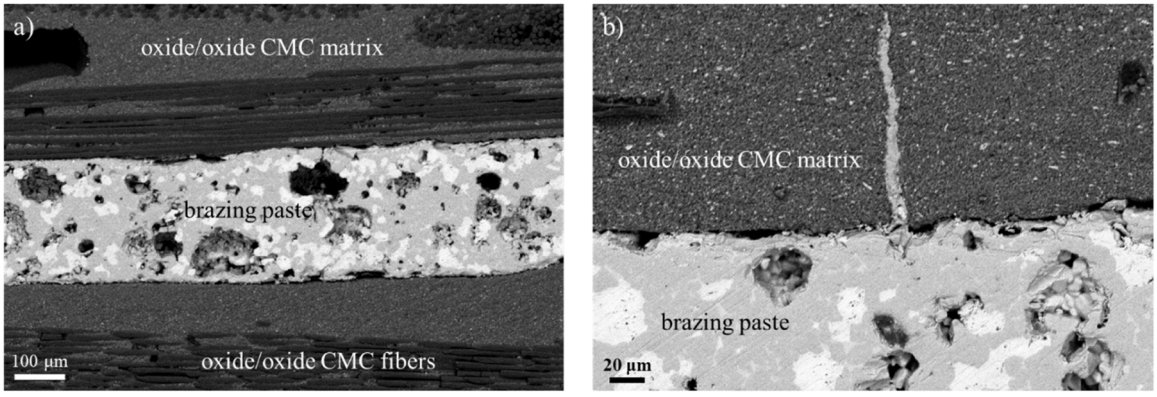

Fig. 5. Cross-sections of the oxide/oxide CMCs joined with TiBraze200Nb brazing paste in the flat-configuration. Image (a) shows the overall view of the brazed joint, while (b) depicts the interface with the oxide/oxide CMC. Both images were obtained in BSE mode.

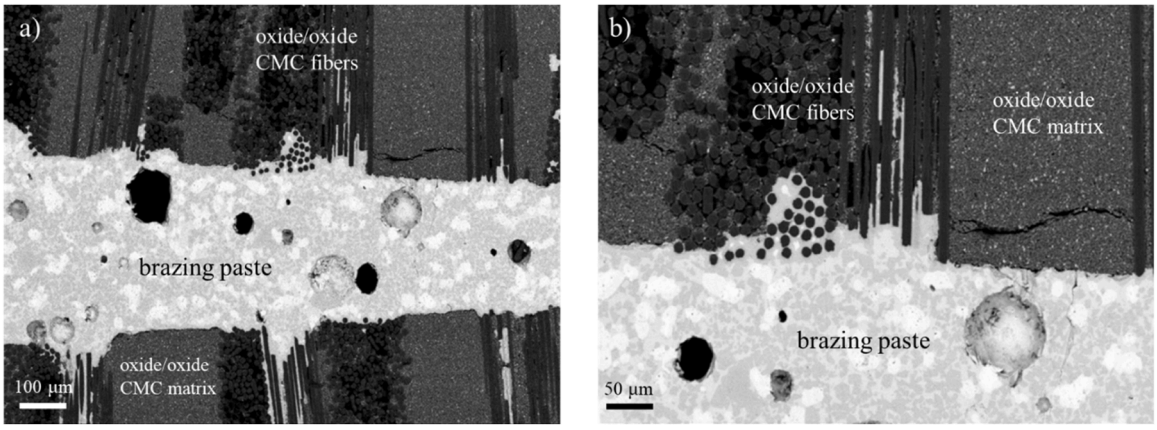

Fig. 6. Cross-sections of the oxide/oxide CMCs joined with TiBraze200Nb brazing paste in the butt-configuration. Image (a) shows the overall view of the brazed joint, while (b) depicts the interface with the oxide/oxide CMC. Both images were obtained in BSE mode.

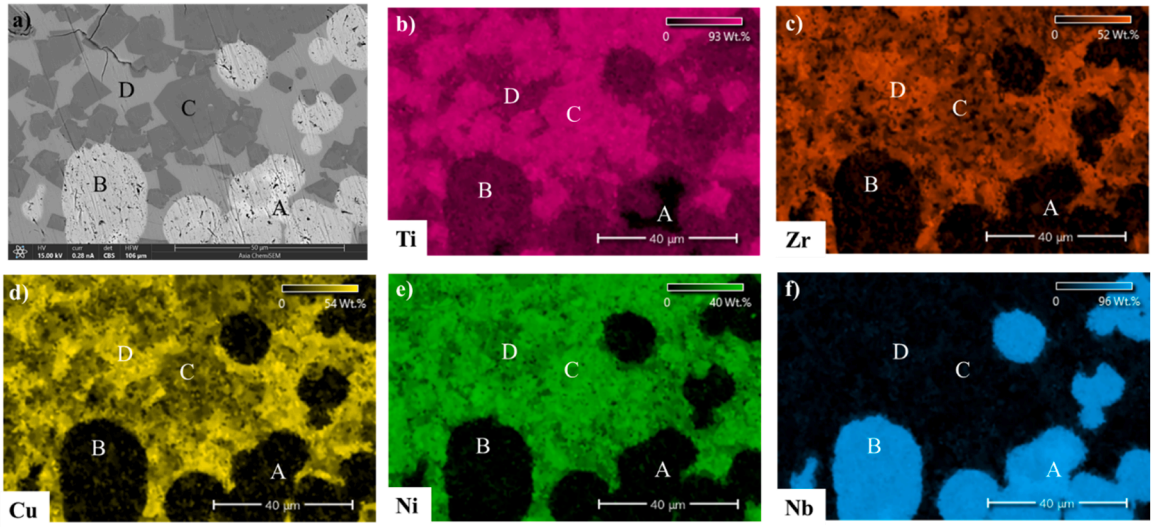

Fig. 7. EDX elemental maps showing the microstructure of the TiBraze200Nb brazing seam obtained with the brazing cycle described. Image (a) shows a high-resolution image of the area of interest, while images (b-f) report the elemental maps of Ti, Zr, Cu, Ni, and Nb respectively.

ref. [40], where in a $(CoCrFeMnNi)_{100-x}Nb_x$ brazing system the presence of Nb increased the yield strength but decreased the fracture strain. In ref. [41], Nb improved the plasticity and the thermal stability of the $Mo_{0.25}V_{0.25}Ti_{1.5}Zr_{0.5}Nb_x$ alloy thanks to the high melting point, but decreased the hardness. The effect of Nb on the corrosion resistance of the alloy was not studied. In ref. [42], Ni and Cu were used as melting-point depressants for Ti-based alloys, while the introduction of Nb eliminated the formation of joint cracks caused by thermal stress.

The light grey phase in area B consisted of a Nb-rich phase alloyed with titanium, indicating the formation of a titanium-niobium phase, due to the dissolution of Nb in Ti. In this regard, ref. [43] reported a TiZrCuNi alloy that was joined to a Nb substrate. A formation of a (Ti, Nb) solid solution phase was observed in the brazing seam, which had a low elastic modulus and good ductility.

The dark grey phase (area C) was attributed to a titanium-rich phase alloyed with Ni as well as lower contents of Cu and Zr contents, while area D could also be attributed to a titanium-nickel-based phase, with higher amounts of copper and zirconium than in area C, as indicated in ref. [26]. A TiZrCuNi filler system and its microstructure were previously studied [44] based on the different compositions of the alloy. In particular, for a Ti–20Zr–20Cu–20Ni system, three distinctive phases, a Ti-rich phase alloyed with low Cu, Ni, Zr contents, a Cu–Ni-rich Ti phase and a Cu–Ni–Zr rich Ti phase, were found. Moreover, the amount of both the Cu–Ni-rich and Cu–Ni–Zr-rich Ti phases decreased with increasing the brazing temperature [26]. The phases obtained after the brazing cycle created a heterogeneous microstructure of the brazed joint, which can be observed by EDX analysis.

High-entropy alloys significantly outperform conventional brazing

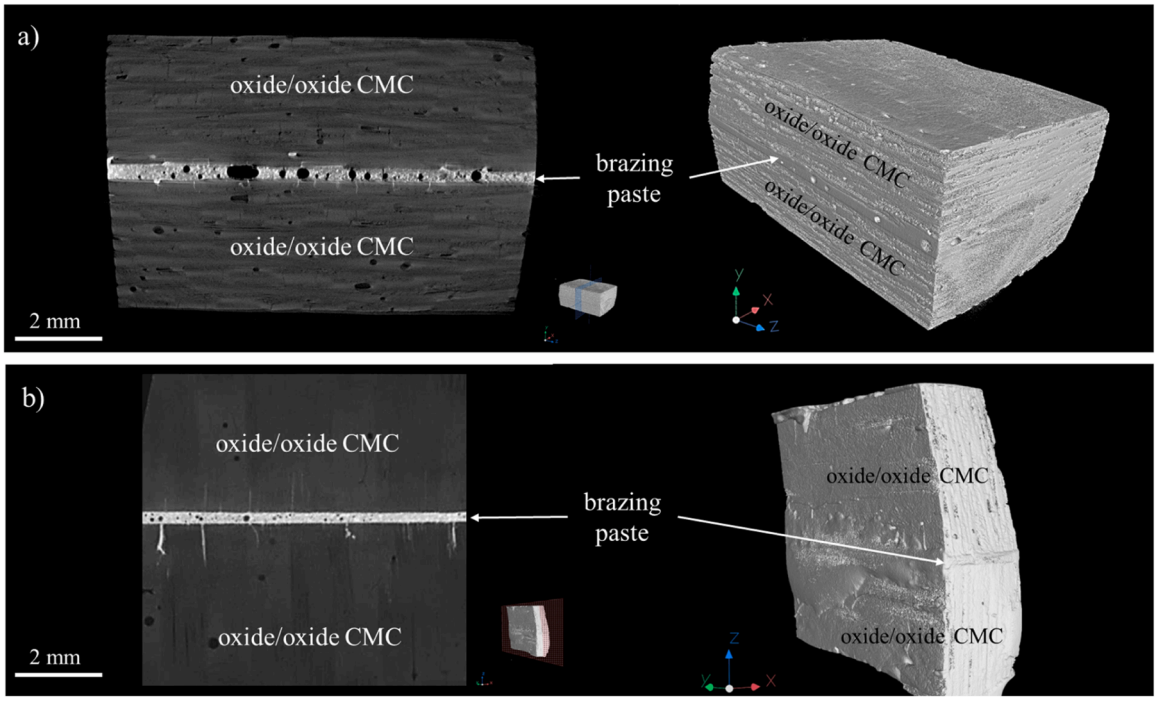

Fig. 8. XCT cross-sections and 3D views of oxide/oxide CMC brazed joint in flat-configuration (a) and in butt-configuration (b). The presence of some voids along the brazing seam can be observed, while the infiltration of the brazing alloy into the CMC is evident in the case of the butt-joint.

alloys by providing refined microstructures, able to minimize cracking and enhance joint integrity as demonstrated in the butt-configurations discussed.

X-ray computed tomography was used to analyse the interface between the brazing alloy and the oxide/oxide CMCs and to investigate the porosity along the brazing seam. A typical joint obtained and the cross-section of the 3D flat-joint sample are reported in Fig. 8a. A few pores are observed within the brazing seam, which can be attributed to the debinding process of the binder in the brazing paste. During debinding, the binder decomposes or evaporates, leaving some voids, which can affect the quality and integrity of the brazed joints. X-ray CT was also performed on the 3D butt-joint sample and the cross-section is shown in Fig. 8b, where the infiltration of the brazing alloy into the composite is clearly visible, promoting the interlocking effect.

The mechanical strength of the joints was evaluated with single-lap offset tests under compression in both flat and butt-configuration joints. Fig. 9 shows the representative shear strength load-displacement curves and the apparent shear strength values obtained for the TiBraze200Nb brazed joints in flat and butt configuration. In the case of butt-joints, the curve showed the pseudo-ductile fracture behavior typical of CMCs, which occurred due to the toughening mechanisms of crack bridging and deflection.

For the flat-configuration, the apparent shear strength of the joints was only 4 ± 2 MPa, while for the butt-configuration the apparent shear strength of the joints was 49 ± 8 MPa.

The value of the apparent shear strength for the flat-joints was lower than the ILSS of the composite (12 MPa), confirming that the worse performance of the flat-joints was caused by the poor adhesion between the brazing alloy and the composite matrix. The worst cohesion was probably caused by the presence of ZrO_2. The flat-joints failed with an adhesive fracture that propagated along the interface with the composite. On the contrary, in butt-joints, the failure was caused by delamination of the upper edge of the composite. The differences in the apparent shear strength mean values and failure mode for the two configurations were likely related to the much better infiltration, excellent wetting and the interlocking between the brazing alloy and the composite along the alumina fibers in the case of butt-joints (Fig. 6b).

The apparent shear strength of brazing alloys as joining materials for oxide/oxide CMCs is relatively little studied. SLO shear tests were performed using AgCuTi, AgCuSnTi, ZrNiTiHf and TiCuAl as brazing alloys for oxide/oxide CMCs (Nextel™ 610/YAG-ZrO_2). In the case of flat-joints, the average shear strength measured was reported between 2 and 5 MPa [16], which was similar to the one measured in this work. For comparison, in ref. [16] a glass-ceramic system was also used to join the oxide-based composite in flat-configuration, achieving an apparent shear strength of 15.4 ± 1.2 MPa.

In another study, two glass-ceramic systems were used to join the same oxide/oxide CMCs employed as in the present study, the apparent shear strengths of flat-joints were measured to be 18 ± 5 MPa and 12 ± 5 MPa, respectively [35]. Compared to glass-ceramics, brazing alloys allow the joining process to be carried out at lower temperatures, i.e. 1050°C with brazing alloys vs. up to 1300°C with glass-ceramics.

To replicate the in-service conditions of the radiant tubes, direct flame exposure tests were carried out on flat and butt-joints, as shown in Fig. 10a for butt-joint configuration. In the case of the flat-joints, the flame treatment duration was 60 min. No damage was observed during the flame test. However, after cooling, the two substrates of the oxide/oxide composites did not adhere to each other, and the joint in this configuration failed to fulfill its function. Due to the failure observed in the previous test, the test duration was reduced from 60 min to 30 min in the case of the butt-joint. It was found that the brazing material was not altered by the flame treatment. Only a slight colour change to black was noted. The bond between the two parts was not affected by the treatment either, and the joint in this configuration survived the test. The cross-section of the butt-joint after the test is shown in Fig. 10b. The failure observed in the flat-configuration joint could be therefore a consequence of the defects initially present at the interface of the composite matrix and the brazing alloy.

To summarize, the oxide/oxide CMCs brazed with TiBraze200Nb brazing alloy with a binder content of 16 wt%, obtained with the brazing cycle reaching up to 1050 °C, resulted into having successful brazed joints, when the butt-configuration is used. They reached a very high value of apparent shear strength and, consequently, delamination of the composite instead of a cohesive or adhesive failure.

4. Conclusions

The application of a titanium-based high-entropy alloy was investigated for brazing oxide/oxide CMCs. The brazing heat treatment was

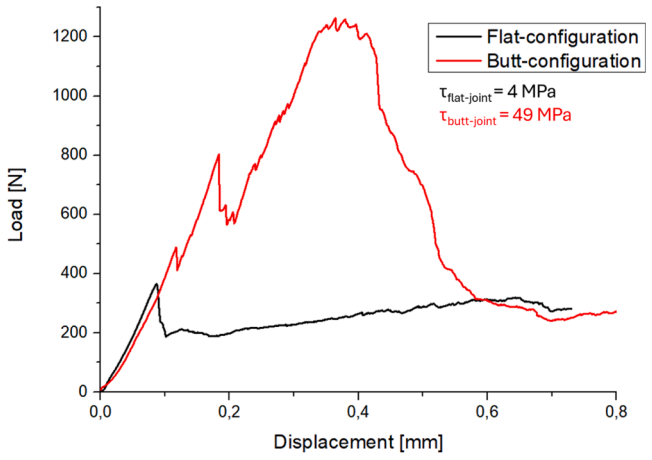

Fig. 9. Representative load-displacement curves obtained from SLO mechanical tests on the oxide/oxide CMCs joined with TiBraze200Nb brazing paste at room temperature in flat-configuration (black curve) and in butt-configuration (red curve). The values of apparent shear strengths obtained are also reported.

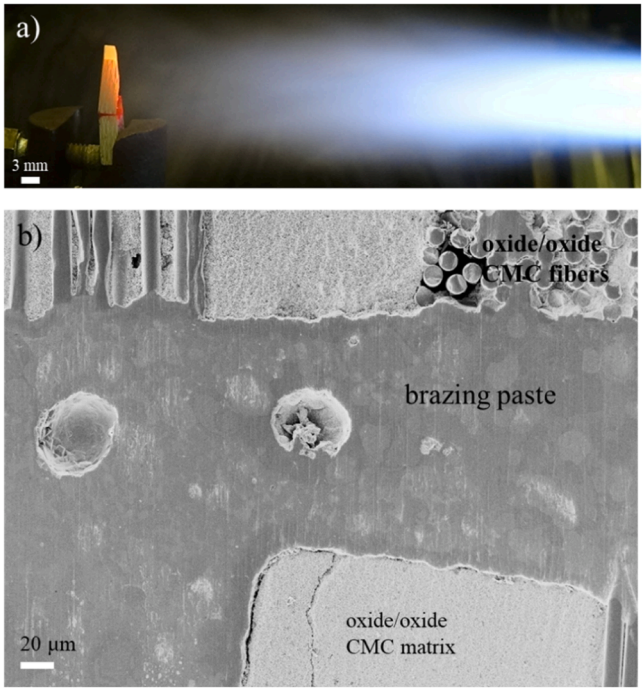

Fig. 10. Direct flame exposure test set-up for the butt-configuration joint (a), and the cross-section of the butt-joint after the flame test (b). The joint survived the test and didn't show modifications in terms of interface adhesion and brazing alloy microstructure.

performed under vacuum (10^{-5} mbar) at temperatures reaching 1050 °C. The TiBraze200Nb alloy, with 16 wt% of binder showed suitable brazeability, resulting in a good joining behavior for oxide-based composites. FESEM imaging showed a good interface and an interlocked structure at the brazing alloy/CMC interface for the butt-joint configuration. Mechanical tests indicated that the brazed butt-joints exhibited higher apparent shear strength compared to the flat-configuration counterparts. Finally, flame tests highlighted the superior performance of butt-joints over the flat-joints when directly exposed to a C_2H_2/O_2 flame at 900 °C.

CRediT authorship contribution statement

Carla Malinverni: Writing – original draft, Investigation, Data curation. **Valentina Casalegno**: Writing – review & editing, Conceptualization, Supervision. **Pierre Bertrand**: Investigation, Writing – review & editing. **Georg Puchas**: Resources, Writing – review & editing. **Stefan Schafföner**: Resources, Writing – review & editing. **Milena Salvo**: Writing – review & editing, Conceptualization, Supervision.

Declaration of Competing Interest

The authors declare that they have no known competing financial interests or personal relationships that could have appeared to influence the work reported in this paper.

Acknowledgements

The research carried out to write this article was funded under the CEM-WAVE project. This project has received funding from the European Union's Horizon 2020 research and innovation program under grant agreement No. 958170. This document only reflects the authors' view. The European Commission is not responsible for any use that may be made of the information it contains.

The authors would like to thank Dr. Alexander Shapiro from Titanium Brazing Inc., Dr. Alice Scarpellini for her help in the FESEM characterization and MSc. Carlotta Carrubba for the help in the experimental activity.

References

[1] X. Zhang, X. Wang, W. Jiao, Y. Liu, J. Yu, B. Ding, Evolution from microfibers to nanofibers toward next-generation ceramic matrix composites: a review, J. Eur. Ceram. Soc. 43 (4) (2023) 1255–1269, https://doi.org/10.1016/j.jeurceramsoc.2022.11.033.

[2] J. Sun, D. Ye, J. Zou, X. Chen, Y. Wang, J. Yuan, H. Liang, H. Qu, J. Binner, J. Bai, A review on additive manufacturing of ceramic matrix composites, J. Mater. Sci. Technol. 138 (2023) 1–16, https://doi.org/10.1016/j.jmst.2022.06.039.

[3] A. Kamal, A.K. Shukla, V.M. Shinde, B.V. Rajasekhar, Microstructure and mechanical properties of C/SiC-niobium alloy (C103) joint brazed with TiCuAg alloy for aerospace applications, Ceram. Int. 49 (17, Part B) (2023) 29265–29273, https://doi.org/10.1016/j.ceramint.2023.06.218.

[4] M. Ferraris, F. Gili, X. Lizarralde, A. Igartua, G. Mendoza, G. Blugan, L. Gorjan, V. Casalegno, SiC particle reinforced Al matrix composites brazed on aluminum body for lightweight wear resistant brakes, Ceram. Int. 48 (8) (2022) 10941–10951, https://doi.org/10.1016/j.ceramint.2021.12.313.

[5] F. Bonzoms, S. Thil, R. Reoyo-Prats, E. Guillot, A. Proust, V. Chaumat, T. Chotard, O. Faugeroux, Thermomechanical characterization of brazed SiC assemblies for receivers of CSP plants, Sol. Energy Mater. Sol. Cells 266 (2024) 112697, https://doi.org/10.1016/j.solmat.2024.112697.

[6] H. Bian, Y. Song, D. Liu, Y. Lei, X. Song, J. Cao, Joining of SiO2 ceramic and TC4 alloy by nanoparticles modified brazing filler metal, Chin. J. Aeronaut. 33 (1) (2020) 383–390, https://doi.org/10.1016/j.cja.2019.03.040.

[7] J.S. Pimenta, A.J.A. Buschinelli, R.M. Nascimento, A.E. do; Martinelli, J. Remmel, Joining of zirconia mechanically metallized with titanium, Cerâmica 56 (2010) 212–221, https://doi.org/10.1590/S0366-69132010000300002.

[8] M. Ferraris, V. Casalegno, Integration and joining of ceramic matrix composites. Ceramic Matrix Composites, John Wiley & Sons, Ltd, 2014, pp. 549–567, https://doi.org/10.1002/9781118832998.ch19.

[9] B. Riccardi, C.A. Nannetti, J. Woltersdorf, E. Pippel, T. Petrisor, Brazing of SiC and SiCf/SiC composites performed with 84Si-16Ti eutectic alloy: microstructure and strength, J. Mater. Sci. 37 (23) (2002) 5029–5039, https://doi.org/10.1023/A:1021087632155.

[10] Z. Wang, M. Yang, H.A. Butt, G. Li, M. Li, H. Li, K. Han, Y. Lei, A novel in-situ forming 3D core-sheath interlayer designed to strengthen Cf/C composite-Nb joints during brazing, Mater. Charact. 208 (2024) 113661, https://doi.org/10.1016/j.matchar.2024.113661.

[11] X. Jiang, G. Zhang, Y. Cao, P. He, G. Yang, Ultra-high temperature brazing of C/C composite using pure Ni as filler based on eutectic reaction, Mater. Lett. 351 (2023) 135006, https://doi.org/10.1016/j.matlet.2023.135006.

[12] C. Malinverni, M. Salvo, M. Ziętara, G. Cempura, A. Kruk, J. Maier, C. Prentice, M. Farnham, V. Casalegno, A yttrium aluminosilicate glass-ceramic to join SiC/SiC composites, J. Eur. Ceram. Soc. 44 (6) (2024) 3579–3587, https://doi.org/10.1016/j.jeurceramsoc.2023.12.095.

[13] J. Wang, G. Yang, F. Zhang, Y. Xiong, Q. Xiong, The preparation and mechanical properties of carbon/carbon (C/C) composite and carbon fiber reinforced silicon carbide (Cf/SiC) composite joint by partial transient liquid phase (PTLP) diffusion bonding process, Vacuum 158 (2018) 113–116, https://doi.org/10.1016/j.vacuum.2018.09.045.

[14] M. Patel, V. Singh, S. Singh, V.V. Bhanu Prasad, Micro-structural evolution during diffusion bonding of C-SiC/C-SiC composite using Ti interlayer, Mater. Charact. 135 (2018) 71–75, https://doi.org/10.1016/j.matchar.2017.11.031.

[15] M. Singh, S.C. Farmer, J.D. Kiser, Joining of silicon carbide - based ceramics by reaction forming approach, Ceram. Eng. Sci. Proc. 18 (3 A) (1997) 161–266.

[16] M.Y. Akram, M. Ferraris, V. Casalegno, M. Salvo, G. Puchas, S. Knohl, W. Krenkel, Joining and testing of alumina fibre reinforced YAG-ZrO2 matrix composites, J. Eur. Ceram. Soc. 38 (4) (2018) 1802–1811, https://doi.org/10.1016/j.jeurceramsoc.2017.11.026.

[17] C. Gadelmeier, J. Schmidt, M. Göthe, D. Jovanovic, Characterization of furnace sintered mullite and oxide ceramic matrix composites (O-CMC) by using glass solders, Adv. Sci. Technol. 88 (2014) 162–171, https://doi.org/10.4028/www.scientific.net/AST.88.162.

[18] C. Gadelmeier, J. Schmidt, D. Jovanovic, M. Zietkowski, C. Eckardt, M. Gorywoda, Adhesive bonding of oxide ceramics for complex ceramic parts in high temperature furnaces, *825–826*, Mater. Sci. Forum (2015) 279–286, https://doi.org/10.4028/www.scientific.net/MSF.825-826.279.

[19] D. Luo, Y. Xiao, L. Hardwick, R. Snell, M. Way, X. Sanuy Morell, F. Livera, N. Ludford, C. Panwisawas, H. Dong, R. Goodall, High entropy alloys as filler metals for joining, Entropy 23 (1) (2021) 78, https://doi.org/10.3390/e23010078.

[20] F. Khan, S.H. Rajendran, J.P. Jung, Recent advances in high entropy alloy fillers for brazing similar and dissimilar materials: a review, Met. Mater. Int. 30 (5) (2024) 1145–1169, https://doi.org/10.1007/s12540-023-01582-9.

[21] Z. He, C. Li, X. Si, J. Qi, J. Cao, Wetting of Si–14Ti alloy on SiCf/SiC and C/C composites and their brazed joint at high temperatures, Ceram. Int. 47 (10, Part A) (2021) 13845–13852, https://doi.org/10.1016/j.ceramint.2021.01.250.

[22] H. Xu, L. Shi, C. Lu, H. Li, Y. He, W. Chen, Y. Li, J. Yang, W. Zheng, Y. Ma, D. Wang, Z. Ding, H. Zou, Z. Gao, A novel joining of Cf/C composites using AlCoCrFeNi2.1 high-entropy brazing filler alloys, Mater. Charact. 179 (2021) 111368, https://doi.org/10.1016/j.matchar.2021.111368.

[23] G. Wang, Y. Yang, M. Wang, R. He, C. Tan, W. Cao, H. Xu, Brazing ZrB2-SiC ceramics to Nb with a novel CoFeNiCrCu high entropy alloy, J. Eur. Ceram. Soc. 41 (1) (2021) 54–61, https://doi.org/10.1016/j.jeurceramsoc.2020.08.050.

[24] A. De Zanet, M. Pedroni, M. Salvo, E. Vassallo, V. Casalegno, Plasma etching as a surface engineering technique for SiC/SiC composites to improve joint strength, Ceram. Int. 49 (7) (2023) 10608–10614, https://doi.org/10.1016/j.ceramint.2022.11.248.

[25] X. Chao, E.-H. Han, Z. Zhang, J. Wang, H. Fu, H. Zhang, G. Hu, Microstructure, mechanical properties and corrosion resistance of the Mo0.5V0.5NbTiZrx high-entropy alloys with low thermal neutron sections, Acta Metall. Sin. Engl. Lett. (2024) 1–14, https://doi.org/10.1007/s40195-024-01728-7.

[26] C. Lin, R.-K. Shiue, S.-K. Wu, H.-L. Huang, Infrared brazing of CoCrFeMnNi equiatomic high entropy alloy using nickel-based braze alloys, Entropy 21 (3) (2019) 283, https://doi.org/10.3390/e21030283.

[27] Shapiro, A.. High-Entropy Brazing Alloys for Joining Refractory Metals; Denver, 2021.

[28] D. Bridges, D. Fieser, J.J. Santiago, A. Hu, Novel frontiers in high-entropy alloys, Metals 13 (7) (2023) 1193, https://doi.org/10.3390/met13071193.

[29] S.A. Krishna, N. Noble, N. Radhika, B. Saleh, A comprehensive review on advances in high entropy alloys: fabrication and surface modification methods, properties, applications, and future prospects, J. Manuf. Process. 109 (2024) 583–606, https://doi.org/10.1016/j.jmapro.2023.12.039.

[30] J.-W. Yeh, Alloy design strategies and future trends in high-entropy alloys, JOM 65 (12) (2013) 1759–1771, https://doi.org/10.1007/s11837-013-0761-6.

[31] W.H. Liu, Y. Wu, J.Y. He, Y. Zhang, C.T. Liu, Z.P. Lu, The phase competition and stability of high-entropy alloys, JOM 66 (10) (2014) 1973–1983, https://doi.org/10.1007/s11837-014-1119-4.

[32] X. Wang, D. Dong, X. Yang, P. Huang, K. Shi, T. Ma, D. Zhu, L. Liu, Microstructure and shear strength of brazing high entropy TiZrHfNbMo alloy and Si3N4 ceramics joints, Crystals 11 (2021) 472, https://doi.org/10.3390/cryst11050472.

[33] Y. Jing, H. Yang, Y. Shang, H. Xiong, The design of a new Ti-Zr-Cu-Ni-Ag brazing filler metal for brazing of titanium alloys, Weld. World 65 (2021) 1–7, https://doi.org/10.1007/s40194-021-01181-5.

[34] G. Puchas, S. Möckel, W. Krenkel, Novel prepreg manufacturing process for oxide fiber composites, J. Eur. Ceram. Soc. 40 (15) (2020) 5930–5941, https://doi.org/10.1016/j.jeurceramsoc.2020.06.064.

[35] C. Malinverni, M. Salvo, A. De Zanet, F. D'Isanto, F. Smeacetto, P. Bertrand, G. Puchas, S. Schafföner, V. Casalegno, Glass-ceramics for joining oxide-based ceramic matrix composites (Al2O3/Al2O3-ZrO2) operating under direct flame

exposure, J. Eur. Ceram. Soc. 43 (8) (2023) 3621–3629, https://doi.org/10.1016/j.jeurceramsoc.2023.02.019.
[36] D.B. Miracle, O.N. Senkov, A critical review of high entropy alloys and related concepts, Acta Mater. 122 (2017) 448–511, https://doi.org/10.1016/j.actamat.2016.08.081.
[37] O.N. Senkov, J.D. Miller, D.B. Miracle, C. Woodward, Accelerated exploration of multi-principal element alloys for structural applications, Calphad 50 (2015) 32–48, https://doi.org/10.1016/j.calphad.2015.04.009.
[38] P. Nikolopoulos, G. Ondracek, D. Sotiropoulou, Wettability and interfacial energies between zirconia ceramic and liquid metals, Ceram. Int. 15 (4) (1989) 201–206, https://doi.org/10.1016/0272-8842(89)90039-4.
[39] J. Zhu, A. Kamiya, T. Yamada, W. Shi, K. Naganuma, K. Mukai, Surface tension, wettability and reactivity of molten titanium in Ti/Yttria-stabilized zirconia system, Mater. Sci. Eng. A 327 (2) (2002) 117–127, https://doi.org/10.1016/S0921-5093(01)01732-4.
[40] G. Qin, Z. Li, R. Chen, H. Zheng, C. Fan, L. Wang, Y. Su, H. Ding, J. Guo, H. Fu, CoCrFeMnNi high-entropy alloys reinforced with laves phase by adding Nb and Ti elements, J. Mater. Res. 34 (6) (2019) 1011–1020, https://doi.org/10.1557/jmr.2018.468.
[41] F. Zhang, C. Xiang, E.-H. Han, Z. Zhang, Effect of Nb content on microstructure and mechanical properties of Mo0.25V0.25Ti1.5Zr0.5Nbx high-entropy alloys, Acta Metall. Sin. Engl. Lett. 35 (10) (2022) 1641–1652, https://doi.org/10.1007/s40195-022-01399-2.
[42] K. Zhao, D. Liu, Y. Song, Z. Hou, X. Song, Joining C/C–SiC composite and Ti60 alloy using a semi-solid TiNiCuNb filler, J. Mater. Res. Technol. 27 (2023) 8073–8083, https://doi.org/10.1016/j.jmrt.2023.11.101.
[43] Y. Sun, J. Zhang, M. Yuan, D. Bai, C. Liu, In-situ stabilized β-Ti in Ti-base alloys to enhance Cf/SiC-Nb heterogenous joint, J. Alloy. Compd. 773 (2019) 217–226, https://doi.org/10.1016/j.jallcom.2018.09.232.
[44] Y. Jing, H. Xiong, Y. Shang, Y. Cheng, Simulation on Ti-based filler and vacuum brazing for TA15 alloy, Weld. World 64 (7) (2020) 1261–1268, https://doi.org/10.1007/s40194-020-00909-z.